Sensors and Actuators B 261 (2018) 144–152

Contents lists available at ScienceDirect

Sensors and Actuators B: Chemical

journal homepage: www.elsevier.com/locate/snb

Multifunctional and miniaturized flexible sensor patch: Design and application for *in situ* monitoring of epoxy polymerization

Yang Yang*, Ke Xu, Thomas Vervust, Jan Vanfleteren*

Centre for Microsystems Technology (CMST), imec and Ghent University, Technologiepark 15, Gent-Zwijnaarde, 9052, Belgium

ARTICLE INFO

Article history:
Received 16 July 2017
Received in revised form
29 November 2017
Accepted 16 January 2018
Available online 3 February 2018

Keywords:
Impedance spectroscopy
Polymers
Polymerization
Interdigital sensor
Miniaturization
Printed circuit board technology

ABSTRACT

Sensor systems capable of *in situ*, continuous impedance measurements are expected to play an important role for a broad spectrum of applications. However, widespread use of these devices is hindered by their current form of separated sensors from bulky, expensive readout instruments. Moreover, the lack of other relevant sensing functionalities on the same system results in an incomplete understanding of the complex physical and chemical changes taking place. In this paper, a miniaturized sensor patch (MSP) with simultaneous impedance and temperature measurements and fully integrated readout is cleverly designed. By using an on-board microcontroller, sensor signal is read out locally and transmitted digitally, eliminating the noise on the signal over the transmission path. The MSP is stable over a wide temperature range (20–180 °C), and in various dielectric mediums (air, epoxies). Moreover, flexible circuit board technology based device fabrication permits further extended functionalities of the patch with off-the-shelf surface mounted devices. The MSPs were successfully applied for monitoring the polymerization processes of two epoxies, demonstrated the potential of the proposed sensor patch as an integrated and multifunctional sensing solution.

1. Introduction

Impedance sensors are devices that can measure the electrical impedance of the material to which it is attached. Since the impedance of the materials are dependent on their physical, chemical and biological properties which may change, devices that carries out continuous, *in situ* and real-time impedance measurements present an exciting opportunity for a broad spectrum of applications, such as monitoring of biological activities in human bodies [1–4], quality control of photovoltaic devices [5,6], strain, pressure and tactile sensing in wearable devices [7–11], production and structural health monitoring of polymeric composites [12,13], chemical sensing [14–16], and so on.

Despite the potential of these devices, they are still under investigation primarily as an analytic tool. At present, impedance measurements are usually carried out in idealized laboratory environment using expensive bulky instruments, combined with cumbersome calibration and cable extension techniques to the sensors [17,18]. To address this challenge, sensor systems with integrated readout circuitry were developed [19–22]. For instance, a low-power impedance-to-digital converter was built on silicon chips for sensor array microsystems towards biological applications [19]. CMOS electrochemical impedance spectroscopy biosensor arrays were designed for detecting various biological analytes [20], and prostate cancer DNAs [21]. A sensor interface integrated circuit (IC) was developed for miniaturized dielectric spectroscopy [22]. However, aforementioned systems still require external benchtop instruments, such as functional generators, clocks, amplifiers, as part of the readout circuitry. Moreover, these devices only measure the impedances of materials. Inclusion of other relevant sensing capabilities onto the same platform would enable simultaneous sensing of multiple parameters, thereof provide a complete picture of the complex biological, chemical, and physical changes taking place.

Herein, we present a flexible, miniaturized sensor patch (MSP) with sensors and integrated readout circuitry. The MSP, fabricated using flexible circuit board technology (FCB), comprises a photo-lithographically patterned interdigital sensor for impedance measurement, off-the-shelf surface mounted device (SMD) for temperature measurements, and a microcontroller unit (MCU) for data processing and communication. Taking advantage of the on-board MCU, which locally processes the data and digitally transmits it, the influence of noise on the data over a long signal path is eliminated. The MSP is capable of capacitance and conductance measurements

* Corresponding authors.
E-mail addresses: yang.yang@ugent.be (Y. Yang), jan.vanfleteren@imec.be (J. Vanfleteren).

https://doi.org/10.1016/j.snb.2018.01.141
0925-4005/

over a wide temperature range (20–180 °C), and in various dielectric mediums (*e.g.* air, epoxies). In addition, the multifunctional MSP was successfully applied for *in situ* and real-time monitoring of epoxy polymerization. The measurements from the MSP indicated the different stages of these processes as confirmed by a reference measurement using a commercial impedance analyzer. This work opens up new design opportunities for impedance sensing devices.

2. Experimental

2.1. Fabrication of the MSP

The fabrication process starts from micro structuring a copper pattern on a flexible PI-Cu (UPISEL-N BE1410, UBE Inc., Japan) substrate *via* photolithography and wet etching. Then, a flexible circuit coverlay with an adhesive layer was laser cut, and laminated on the micro structured circuit at 120 °C. Afterwards, organic solderability preservative was applied to the copper surface. The lead-free solder paste (DP5505, Interflux, material: Sn96.5Ag3Cu0.5) was dispensed manually using a dispensing system (UltraSaver, EFD Inc, USA) and the chips were assembled manually, and they were afterwards soldered in a reflow oven (IBL SLC300, Siemens). The interdigital sensor (IDS), the calibration unit and the temperature IC (LMT87, Texas Instruments, USA) were built around a MCU (ATmega1280, Atmel, San Jose, USA) with an internal 10-bit analog to digital converter (ADC). A temperature insensitive SMD capacitor of 22 pF (1% precision, 0 temperature drift) was connected to MCU as the calibration unit.

2.2. In situ *monitoring of two epoxies*

Two epoxy systems were studied. The epoxy system (Sicomin, Châteauneuf-les-Martigues, France) is a two-part system comprising the resin (SR8500) and the hardener (SZ8525). The epoxy system (Momentive, Waterford, NY, USA) is a two-part system comprising the resin (EPIKOTE MGS RIMR 135) and the hardener (EPIKURE MGS RIMH 137). For both epoxies, 100 g of resin and 30 g of hardener were thoroughly mixed and degassed. A MSP, a reference IDS (design: $W = g = 100$ μm, $L = 15$ mm, and 40 fingers) and a reference thermocouple (type K) were placed closely together on a polydimethylsiloxane mould. Afterwards, the resin mixture was slowly poured into the mould until completely covering the MSP, the reference IDS, and the thermocouple. RIMR135 resin was cured for 40 h at room temperature (22 °C), SR8550 were cured at 70 and 90 °C. An HP 4284A Precision LCR meter performed the impedance measurement of the IDS with frequency sweep ranging from 100 Hz to 1 MHz with 10 points per decade. A thermocouple data logger TC-08 (Pico Technology, UK) was used for the temperature measurements. The time required per sweep was 5 s for the MSP, 16 s for the LCR meter, and 5 s for the thermocouple data logger.

3. Design of the miniaturized sensor patch (MSP)

3.1. System overview

Novel impedance sensing devices are aimed to be applied in-field or in-body to permit real-time and *in situ* monitoring functionalities. Hence, for these types of devices to be useful, compact designs with integrated readout are desirable. Fig. 1a shows an example of *in situ* structural health monitoring of a polymeric composite material using the MSP, where different sensors are integrated in a single platform for multifunctional sensing, such as impedance (capacitance, conductance) and temperature measurements. The sensor patch should be flexible, small-sized, and light-weight to minimize its disturbance to the integrated structure [23–25]. Fig. 1b illustrates the system-level block diagram of the proposed MSP. The MSP uses an interdigital sensor (IDS) employing a readout circuitry and a calibration unit for accurate impedance measurements and a commercial temperature IC for temperature measurement. The IDS, the calibration unit and the temperature IC are built around a microcontroller unit (MCU) with a 10-bit analog to digital converter (ADC). Thanks to the on-board MCU, virtually all commercial sensor ICs can be incorporated to the MSP to further extend its functionalities. An on-board multiplexer (MUX) switches between the IDS and calibration unit to the ADC. The microcontroller's serial communication capability is used to transmit the data to the PC's virtual serial port through USB. The MSP is powered by an external voltage source of 5 V. Its power consumption depends on the MCU in use. The MCU in its present setup consumes 10 mA, with an input voltage of 5 V and running at 8 MHz, as stated in the datasheet. A photograph of the fabricated MSP, with a size of 24 mm × 20 mm, is shown in Fig. 1c.

The flow chart of the overall measurement scheme of the MSP is illustrated in Fig. 1d. First, the MCU is initialized with hardware configurations. Then, the program selects the first channel, i.e. the channel with the IDS. The program reads the ADC value and stores it in the data register; next, the program selects the second channel, the one with the calibration unit, and the same procedure is repeated. Afterwards, the program proceeds to the temperature measurement IC. Finally, all the data are sent to the PC in one go, and the MCU loops back after a programmed delay. One complete cycle takes about 5 s, which is programmable depending on the actual measurement scenario. Further details on the impedance measurement is discussed in next section.

3.2. Operating principles of the impedance measurements

3.2.1. Modelling of the impedance readout circuitry

We propose a simple yet effective readout circuitry capable of rapid and accurate capacitance and conductance measurements over a wide temperature range (20–180 °C), and in various dielectric mediums (*e.g.* air, epoxies). Fig. 2 depicts the operating principle of the impedance measurement of the MSP. The readout circuitry (Fig. 2a), termed the bridge in this article, is built around the MCU. The upper side of the bridge represents the IDS with a capacitance of C_{MUT}, and the lower side represents a reference capacitance of C_S. The lossy part of the capacitor is modeled as a parallel resistor, where R_{MUT}, R_S is the lossy part of C_{MUT} and C_S, respectively. An interdigital sensor, as shown in Fig. 2b, operated in the fringing electric field mode as demonstrated by the finite element modelling, is designed for impedance sensing. In an IDS structure, L, W, g, N, η, stands for the length of the finger, width of each finger, the spacing between fingers, the number of fingers, and the metallization ratio ($\eta = W/(W+g)$), respectively. These geometrical parameters are important factors that influence the sensor's nominal value and sensitivity [26]. In the section 'design consideration', further details on how to select the design parameters will be discussed. We start with both capacitors discharged and both input and output pin at 0 V. When a voltage, $v_{IN}(t)$, is supplied at the input, a current will flow through both capacitors. $v_{IN}(t)$As a result, the output voltage, $v_{OUT}(t)$, will respond in accordance to $v_{IN}(t)$. $v_{OUT}(t)$ is a function of, $v_{IN}(t)$, C_{MUT}, C_S, R_{MUT}, and R_S. By establishing the input-output relationship of the system, the system parameters of the circuit can be extracted. Here, the circuit is first analyzed in s-domain using Laplace transform for the sake of simplicity [27], and then converted to time domain using inverse Laplace transform. From Kirchhoff's current law, we have:

$$sC_{MUT}(V_{IN} - V_{OUT}) + \frac{V_{IN} - V_{OUT}}{R_{MUT}} = sC_S V_{OUT} + \frac{V_{OUT}}{R_S} \quad (1)$$

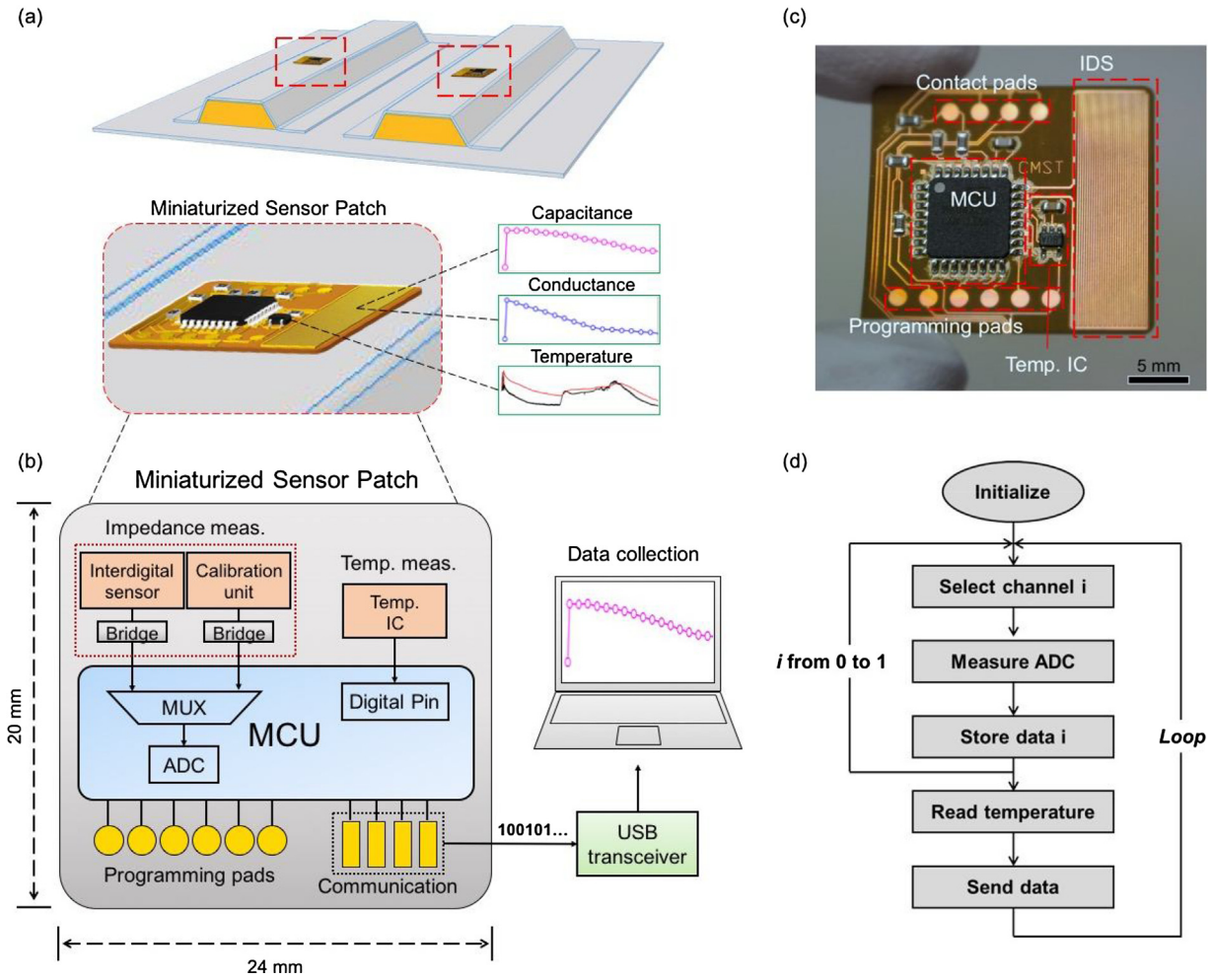

Fig. 1. Overview and system design of the proposed flexible, multifunctional, miniaturized sensor patch (MSP): (a) Schematic of the MSP embedded in a polymeric composite structure for *in situ* monitoring of its production process. (b) System-level block diagram of the MSP showing the interdigital sensor and calibration unit for impedance measurement, temperature sensor, microprocessor for data processing and communication, wired transmission path, and the PC for data collection. (c) Photograph of the fabricated MSP. (d) Simplified flowchart of the overall measurement scheme.

Re-arranging the equation, we obtain the system's transfer function$H(s)$:

$$H(s) = \frac{V_{OUT}(s)}{V_{IN}(s)} = \frac{sC_{MUT} + 1/R_{MUT}}{s(C_{MUT} + C_S) + \left(1/R_{MUT} + 1/R_S\right)} \tag{2}$$

After partial fraction expansion, we have:

$$H(s) = \frac{C_{MUT}}{C_{MUT} + C_S} + \frac{C_s/R_{MUT} - C_{MUT}/R_S}{(C_{MUT} + C_S)^2 s + (C_{MUT} + C_S)\left(1/R_{MUT} + 1/R_S\right)} \tag{3}$$

A square wave is supplied at the input with amplitude of V_{CC} and duration of T_1, i.e.:

$$v_{IN}(t) = V_{CC}(u(t) - u(t - T_1)) \tag{4}$$

where $u(t)$ is the Heaviside step function, whose value is zero for negative argument and one for positive argument. $u(t - T_1)$ stands for the Heaviside step function that is shifted T_1 in time axis. We obtain the s-domain equivalent of $v_{IN}(t)$ through the Laplace Transform (L):

$$V_{IN} = L\left\{V(u(t) - u(t - T_1))\right\}(s) = V_{CC}\left(\frac{1}{s} - \frac{e^{-T_1 s}}{s}\right) \tag{5}$$

Finally, $v_{OUT}(t)$ is calculated using the inverse Laplace transform $\mathcal{L}^{-1}\{H(s)V_{IN}(s)\}(t)$:

$$v_{OUT}(t) = \frac{V_{CC}}{(C_{MUT} + C_S)(\frac{1}{R_{MUT}} + \frac{1}{R_S})}\{[\frac{C_S}{R_{MUT}}(1 - e^{-\frac{t}{\tau}}) + C_{MUT}(\frac{1}{R_{MUT}} + \frac{1}{R_S}e^{-\frac{t}{\tau}})] - [\frac{C_S}{R_{MUT}}(1 - e^{-\frac{t-T_1}{\tau}}) + C_{MUT}(\frac{1}{R_{MUT}} + \frac{1}{R_S}e^{-\frac{t-T_1}{\tau}})]u(t - T_1)\} \tag{6}$$

where the term between the first square bracket describes the behavior of output in response of input signal, and the second describes the exponential decaying of the signal after the input voltage is reset to 0. τ is defined as the time constant of the system:

$$\tau = (C_{MUT} + C_S)/\left(\frac{1}{R_{MUT}} + \frac{1}{R_S}\right) \tag{7}$$

The built-in ADC of the MCU converts the measured voltage, $v_{OUT}(t)$, to a 10-bit digitalvalue, ADC counts, with respect to the analog voltage reference, V_{REF}. The relationship between them is:

$$v_{OUT}(t) = \frac{ADC\ counts}{1024} V_{REF} \tag{8}$$

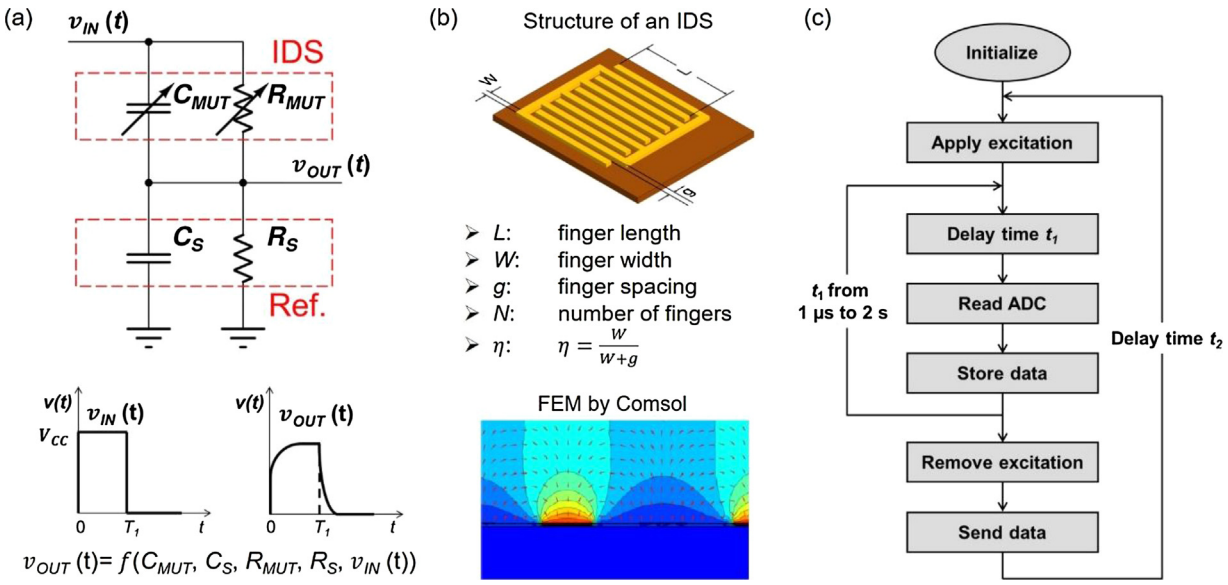

Fig. 2. Operating principle of the impedance measurements: (a) Circuit model of the readout electronics. (b) Structure of an interdigital sensor and its operation principle by the fringing electric field effect. (c) Simplified flowchart shows the scheme of the impedance measurements.

Since the analog voltage reference is internally connected to the input, thus $V_{REF} = V_{CC}$. Inserting Eq. (8) to Eq. (6), we obtain:

$$ADC\ counts = \frac{1024}{(C_{MUT}+C_S)\left(\frac{1}{R_{MUT}}+\frac{1}{R_S}\right)} \left\{\left[\frac{C_S}{R_{MUT}}\left(1-e^{-\frac{t}{\tau}}\right)+C_{MUT}\left(\frac{1}{R_{MUT}}+\frac{1}{R_S}e^{-\frac{t}{\tau}}\right)\right] - \left[\frac{C_S}{R_{MUT}}(1-e^{-\frac{t-T_1}{\tau}})+C_{MUT}\left(\frac{1}{R_{MUT}}+\frac{1}{R_S}e^{-\frac{t-T_1}{\tau}}\right)\right]u(t-T_1)\right\} \quad (9)$$

3.2.2. Software implementation of the MSP

The software implementation of the impedance measurement is shown in Fig. 2c. First, the MCU is initialized with hardware configurations. Then, an excitation voltage is supplied at the input. The software pauses for a programmed time t_1 and reads the ADC, the read value is then stored in a data register. Afterward, the software loops back and the pause-read ADC-store data procedure is repeated until the programmed time elapsed. Finally, the excitation is removed from the input, a delay time t_2 is added before the start of the next measurement to ensure both capacitors are fully discharged. Each measurement loop is determined by the sum of t_1 and t_2. In the current implementation, a cycle time of 2.5 s is programmed (5 s for both the IDS and the calibration unit).

3.2.3. Design considerations of the MSP

Different choices of the reference capacitance C_S would result in different ADC counts. Fig. 3a shows the predicted C_{MUT} as a function of ADC counts (ADC count is proportional to measured voltage) regarding different C_S. For instance, when C_{MUT} = 10 pF, ADC equals to 512, 341, 205 for C_S = 10, 20, 40 pF, respectively. In Fig. 3b, change in ADC counts ($\Delta ADC\ counts$) in function of C_S for three measurement ranges, [10 20] pF, [20 40] pF, and [30 60] pF, are plotted. $\Delta ADC\ counts$ is the difference between minimum and maximum value in each range. The determined best C_S for above-mentioned ranges are 14, 28, 42 pF, respectively, and the corresponding $\Delta ADC\ counts$ all equal to 175. The corresponding resolutions equal to 0.06, 0.11, 0.17 pF. Therefore, C_S should be selected based on the expected measurement range of C_{MUT}, resulting in a maximum

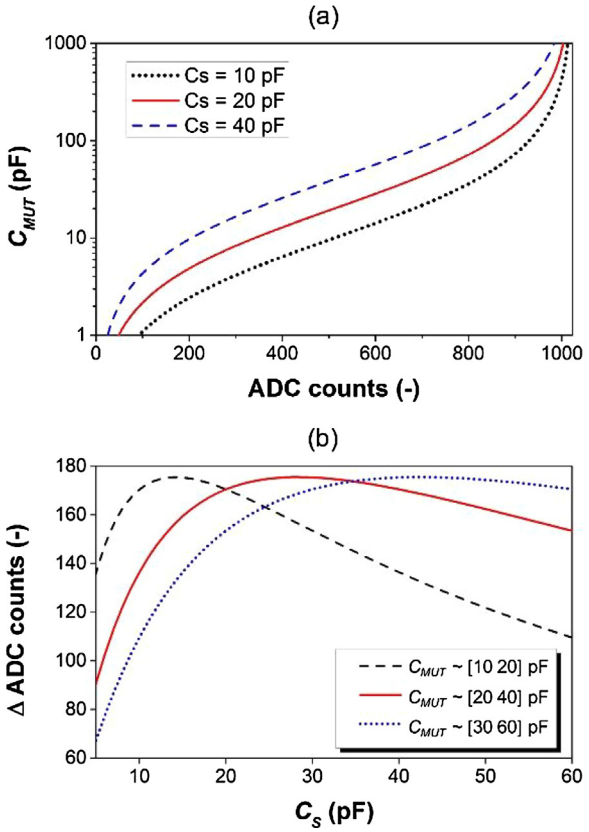

Fig. 3. (a) Predicted C_{MUT} in function of ADC value with different C_S in the bridge. (b) Expected ΔADC as a function of C_S for different intended measurement range.

usage of the ADC range. It is worth mentioning that a smaller range, i.e. increased resolution, can be achieved when a smaller C_S is used. A smaller measurement range of the IDS corresponds to a smaller sensor design [28]. Therefore, the miniaturization of the sensor is possible when a smaller C_S is used. Since the MCU has a stray capacitance of about 21 pF, this is the minimum value for C_S. We will use the stray capacitance of MCU as the C_S instead of physically putting a C_S in the readout circuitry. It should be noted that this method is

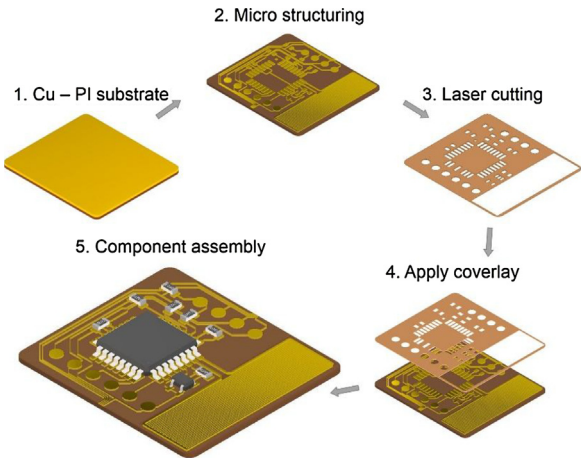

Fig. 4. Schematic representation shows the fabrication steps of the MSP: (1) start from Cu-PI substrate, (2) micro structuring through photolithography and wet etching for creating the sensor and circuit pattern, (3) laser cutting of the flexible circuit coverlay layer, (4) lamination of flexible circuit coverlay with cutout onto the flexible circuit board, (5) assembly of the components onto the flexible circuit board.

only valid if the stray capacitance of the MCU is stable, and consistent, which was found out to be true from our experiments. Further details on this will be discussed later.

An interdigital sensor, which combines geometrical stability, and the possibility to access the MUT (Material Under Test) from one side [29–31], is part of the MSP and used as the sensor for the complex impedance sensing. Based on the value of $C_S \approx 21$ pF, the capacitance of the IDS was designed to fall between [10 40] pF during epoxy curing. To miniaturize the sensors with the desired measurement range, the unit area sensitivity of the sensor to the changing dielectric properties should be maximized. Based on our previous studies [13,28], the maximal unit area sensitivity of the sensor, within our fabrication limit, is achieved with $W = g = 0.1$ mm. The number of fingers, N, and the length of the finger, L, only contribute to the total sensitivity but not to the unit area sensitivity of the sensor, thus can be chosen with more freedom. Bearing in mind the desired range of [10 40] pF, and the board layout of the MSP, the final IDS design was determined to be $W = g = 0.1$ mm, $N = 30$, $L = 20$ mm. The size of the IDS is 120 mm^2, and its sensitivity, or unit area sensitivity is 4.46 pF, 0.025 pf/mm^2 respectively.

3.3. Fabrication of the MSP

The fabrication of the MSP, as shown in Fig. 4, is based on flexible printed circuit board technology [32]. The process is compatible with printed circuit board technology, taking full advantages of existing off-the-shelf SMDs in combination with various chip attachment and assembly methods. The process starts from micro structuring a copper pattern on a flexible polyimide (PI) substrate *via* photolithography and wet etching. PI is used as the substrate material because of its relatively stable electrical, thermal and mechanical properties over a wide temperature and frequency range. Then, a flexible circuit coverlay with an adhesive layer was laser cut, and laminated on the micro structured circuit at 120 °C. The flexible coverlay serves the same function as the soldermask that is used on a rigid printed circuit board to protect the MSP against oxidation and to prevent solder bridges from forming between closely spaced solder pads. Then, organic solderability preservative was applied to enhance the solderability of the copper surface during the next step. At last, passive components, the MCU, and the temperature measurement IC were assembled. The fabricated MSP features an area of 24 mm × 20 mm, an overall thickness of 67 μm (Cu: 17 μm, PI: 50 μm), and 1 mm in the area with the MCU. An analog temperature measurement IC was connected to the MCU for temperature measurement. A temperature-insensitive precision SMD capacitor of 22 pF was connected to MCU as the calibration unit.

4. Results and discussion

4.1. Verification of the measurement principle

To validate the operating principle and implementation of the MSP, capacitors and resistors with known values were assembled around the MSP according to Fig. 2a. Fig. 5 shows the time domain response of $v_{OUT}(t)$ with respect to square wave input $v_{IN}(t)$ for different R-C configurations. The combinations of resistors and capacitors were selected to match the time constant of the system between 2 μs and 2 ms using Eq. (7). The solid curves are the estimated responses using Eq. (6), the blue circles are the obtained measurements from the MSP. The data follow nicely with the model. For instance, as shown in Fig. 5a, the system behaves as a capacitive bridge when the measurement is done sufficiently shortly after the transient response, i.e., when $t \to 0$, Eq. (6) is reduced to:

$$v_{OUT}(t) \approx \frac{C_{MUT}}{C_{MUT} + C_S} V \tag{10}$$

and behaves as a resistive bridge when $t > 3\tau$ & $t < T_1$, $e^{-t/\tau} \approx 0$, Eq. (6) is reduced to:

$$v_{OUT}(t) \approx \frac{R_S}{R_{MUT} + R_S} V \tag{11}$$

The transition time of the system from capacitive to resistive bridge is positively correlated to the time constant of the system. The resistive bridge zone of the system can always be captured by the MSP by increasing the length of the input pulse. On the other hand, to capture the capacitive-bridge zone, the time constant of the system should be significantly larger (100 times larger) than the minimum time required by the MCU to implement the instructions, which is proportional to the system clock of the MCU. The MCU used in this study has a clock speed of 8 MHz, therefore the theoretical minimum measurement time is in the order of sub-microseconds. Taking into account the software commands usually take a few clock cycles, the realistic minimum measurement time is about 1 μs. For example, in Fig. 5a, the measurement covers the complete capacitive-transition-resistive zone, while in Fig. 5b, the tail of the capacitive zone, and transition-resistive zone were covered, in Fig. 5c, only the transition-resistive zones, and in Fig. 5d, the tail of the transition zone and the resistive zone were covered. For a reactive polymer, its complex dielectric properties, extracted from measured complex impedance, change over the polymerization. The time constant of the reactive system, when it is considered in the bridge system of the MSP, is dominated by its equivalent resistance. Throughout the polymerization, the equivalent resistance of the polymer changes about 6 orders of magnitude, whereas its capacitance changes less than 1 order of magnitude. Further results on using the developed MSP on reactive polymers is discussed in Section 4.

4.2. Characterization of the MSP

As previously discussed, we will use the stray capacitance of the MCU as the C_S in the bridge instead of physically putting a capacitor. This method is only valid if the stray capacitance of the MCU is stable, and consistent between different MCUs. To test this, the C_{MUT} in the bridge was replaced by known capacitors. Using Eq. (8), we were able to calculate the actual C_S. 14 MSPs, each with four analog

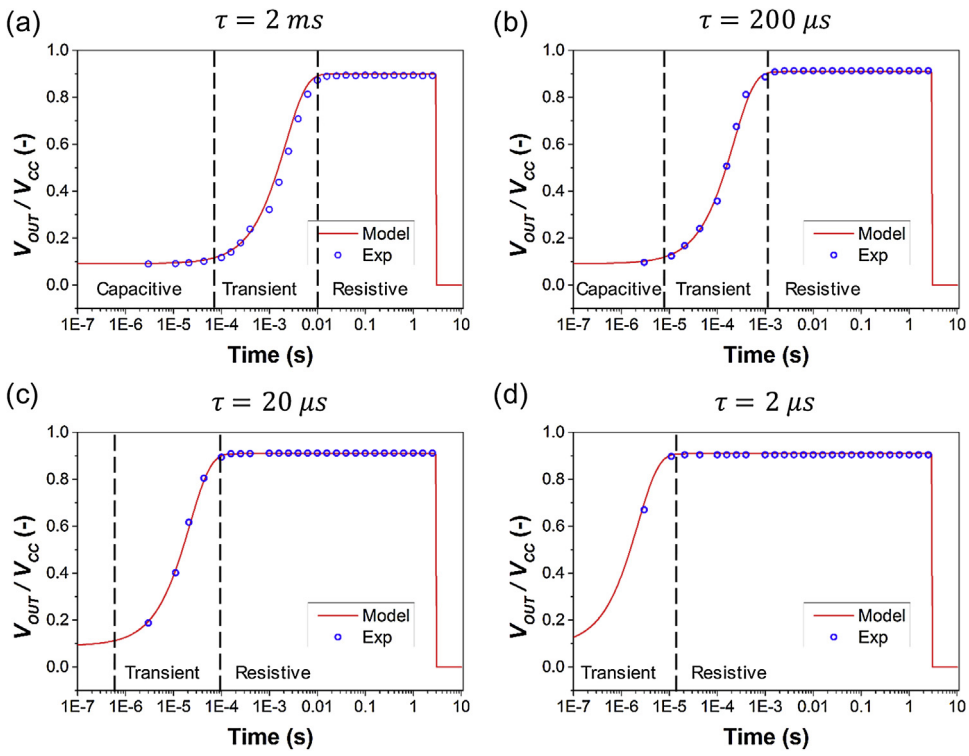

Fig. 5. Time domain responses of v_{OUT} (t) normalized to input amplitude V for different R-C configurations. The solid curves are the estimated response by Eq. (6), the blue circles are the experimental results. (a) C_{MUT} = 220 pF, C_S = 22 pF, R_{MUT} = 10 MΩ, R_S = 89 MΩ. (b) C_{MUT} = 220 pF, C_S = 22 pF, R_{MUT} = 1 MΩ, R_S = 10 MΩ. (c) C_{MUT} = 220 pF, C_S = 22 pF, R_{MUT} = 100 kΩ, R_S = 1 MΩ. (d) C_{MUT} = 220 pF, C_S = 22 pF, R_{MUT} = 10 kΩ, R_S = 100 kΩ. (For interpretation of the references to colour in this figure legend, the reader is referred to the web version of this article.)

Table 1
Details on the consistency of the stray capacitance of the MSP. Results were obtained with a sample size of 14. Four analog ports (A0-A3) of the MSP were tested.

Port	C_S (pF)
A0	20.8 ± 0.8
A1	20.9 ± 0.8
A2	21.0 ± 1.0
A3	21.1 ± 1.0

Table 2
Details on the accuracy of capacitance measurement of the MSP in the range of 10–100 pF.

Nominal capacitance (pF)	Measured value (pF)	Error (pF)	Relative error (%)
10	10.30	0.30	3.0
15	15.08	0.08	0.5
22	21.95	−0.05	−0.2
33	33.09	0.09	0.3
47	46.66	−0.34	−0.7
68	67.32	−0.68	−1.0
100	98.49	−1.51	1.5

pins (A0 to A3), were connected to temperature-independent precision capacitors (0 temperature drift, 22 pF nominal value with 1% error) to calculate C_S. The results at room temperature are shown in Table 1. The results indicate that the stray capacitance of the MCU is quite consistent with a value of 21.0 ± 0.9 pF. Between different analog pins of each MCU, the variance is small, as they are connected to the same ADC through the on-board multiplexer. To conclude, the stray capacitance of different MCUs, and between different analog pins of each MCU is very consistent.

After validating the consistency of the stray capacitance, the accuracy of the MSP for capacitance measurement was investigated. Temperature independent precision capacitors (0 temperature drift, 1% error), as the C_{MUT} in the bridge, in the range of [10 100] pF were built around the MSP and tested. The results are summarized in Table 2. An overall relative error of less than 3% is seen in the range of [10 100] pF.

Temperature dependence of the C_S and R_S was tested by replacing the IDS with a temperature insensitive precision capacitor (0 temperature drift, 22 pF nominal value with 1% error). The results, obtained from the time domain response of v_{OUT} (t) with respect to a square wave input v_{IN} (t) at specified temperatures (Supplementary Material Fig. S1), are shown in Fig. 6a. C_S changes from 20.4 to 20.0 pF when the temperature increases from 30 to 120 °C. On the other hand, the R_S increases almost logarithmically with increasing temperature. In addition to the wide temperature range of the MSP, the MSP has proved to be reliable over a 17 h cycle at 120 °C (see **Fig. S2** in the Supplementary Material).

To test the stability of the MSP for use in a liquid polymer, precision capacitors (22 pF with 1% error), were inserted in the bridge as the C_{MUT}. Fig. 6b shows the ADC readout of the MSP before and after immersing in a room temperature (22 °C) liquid epoxy (RIMR135 + RIMH137). As can be seen, the ADC counts on the capacitive zone remains unchanged after immersing in epoxy. As a result, the calculated C_S remains nearly constant (20.4 pF to 20.7 pF). On the contrary, the curve diverges when the transient time is increased, showing a change in the resistive zone of the bridge. The calculated R_s decreases from 692 GΩ to 9 GΩ. The result suggests that the stray capacitance of the MCU remains constant even in contact with a liquid epoxy, enabling a simple method to calculate the C_{MUT} using Eq. (8). On the other hand, R_s is both dependent on the temperature and the medium in contact. Therefore R_s can only be obtained using Eq. (6).

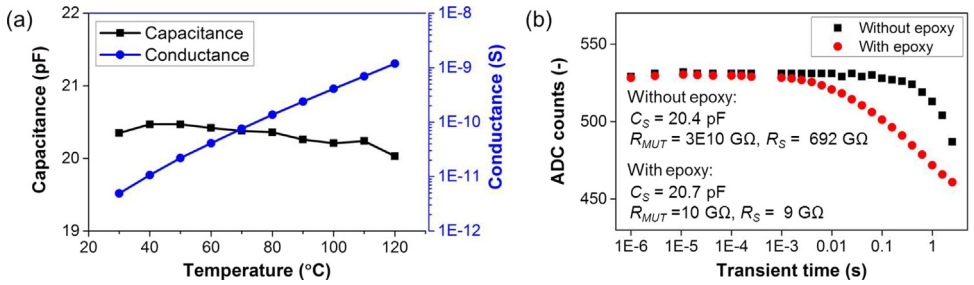

Fig. 6. (a) Temperature dependence for the impedance measurement: Calculated C_S and $G_S(G_S = 1/R_S)$ between 30 and 120 °C. (b) Stability of the MSP for use in a liquid polymer. Calculated parameters without epoxy are: C_S = 20.4 pF, R_{MUT} = 3E10 GΩ, R_S = 692 GΩ; parameters with epoxy are: C_S = 20.7 pF, R_{MUT} = 10 GΩ, R_S = 9 GΩ.

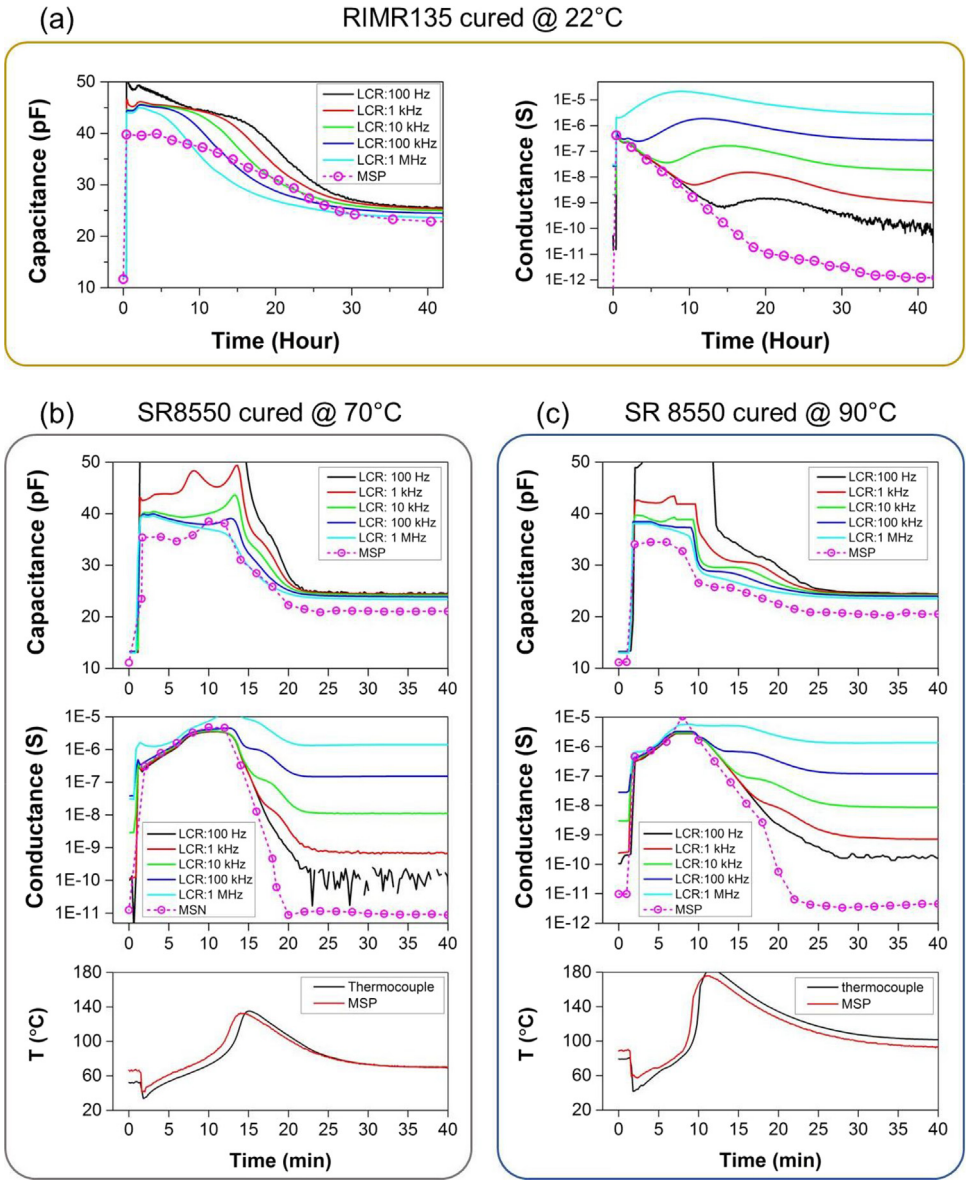

Fig. 7. Real-time and *in situ* monitoring of two epoxy polymerization using the developed MSP compared to IDS + LCR meter: (a) Evolution of complex impedance for RIMR135 cured at 22 °C, (b) SR8550 cured at 70 °C, (c) and SR8550 cured at 90 °C.

4.3. In situ *monitoring of epoxy polymerization using the MSP*

Epoxy is one important polymer material that is extensively used in many industrial applications, such as aerospace, wind energy, automotive, construction. Polymerization of epoxy is a complex process, during which the material undergoes dramatic chemical, and physical changes [33,34]. To ensure the quality of epoxy matrix composites, and improve energy efficiency for the production process, monitoring of the polymerization process is important. Starting materials for epoxy are low molecular-weight organic liquid resins which contain permanent dipole groups and ion species that align with the external electric field. During the

cross-linking of polymer chains, a 3D polymer network is formed, accompanied by the increased resin viscosity, and glass transition temperature [35]. The resulting changes of the measured capacitance, and conductance from an external electric field, provide the basis of impedance spectroscopy for the monitoring of reactive polymers.

In this work, the polymerization processes of two commercial epoxy resins: RIMR135 and SR8550 were studied. *In situ* real-time capacitance and conductance measurements, from both the developed MSP and IDS + LCR meter, are shown in Fig. 7. The circles are the results from the MSP, and the solid curves are the results from the LCR meter. The results of the MSP were obtained from the time domain response of $v_{OUT}(t)$ with respect to a square wave input $v_{IN}(t)$. Further details are available in Supplementary Material Fig. S3.

At the beginning of the experiment, large increases in capacitance (from ~10 pF to ~40 pF) and conductance (from 10E-12 to 10E–6 S) from both measurements, due to the change of MUT from air to liquid epoxy, were seen when the resin flowed over the sensor, as shown in Fig. 7a. At the early stage of the polymerization, migrational ions were capable of travelling between the sensor electrodes due to the low viscosity of the resin. Electrode polarization phenomena occur [36], leading to higher capacitance at lower frequencies (from the LCR meter). This phenomenon is more visible in Fig. 7b and c, where the mobility of the ions was enhanced at higher temperatures. The capacitance measurement of the MSP was slightly lower than 1 MHz measurement of the LCR meter, since the capacitance in the MSP was measured using a square wave input (with a rise time of 6.7 ± 1.2 ns measured by the oscilloscope), which had a higher equivalent frequency than that of the LCR meter. In the meanwhile, the conductance of the resin was dominated by the ionic conductivity, proven by the similar conductance measurements for both the MSP and the different frequencies from the LCR meter for all the experiments. Since the ionic conductivity was a DC component, the measurements between the MSP and the LCR meter were the same despite the differences in measurement principles. Unlike the monotonically decreasing trend of capacitance and conductance seen in Fig. 7a, increases of them were seen in Fig. 7b and c, due to the temperature rise, since the dielectric properties of polymers are known to be temperature dependent. The selectivity of the MSP is crucial, because temperature variance during epoxy polymerization can affect the sensor readings. Supplementary Material Fig. S4 shows that the temperature dependence of impedance measurement for fully cured epoxy over the temperature range of 30–110 °C is far less pronounced compared to the polymerization process itself. During the curing of the resin, cross-linking of polymer chains resulted in the growth of a polymer network with higher molecular weight. A higher molecular weight means more entanglement at the molecular level, and higher viscosities, leading to a restricted ionic diffusion. Electrode polarization disappeared from higher frequencies to lower frequencies. The restricted ion mobility also led to the stepwise decrease of conductance. And at higher frequencies from the LCR meter, the equivalent conductance diverged from the decreasing trend of ion conductance.

Along with the curing progress, the T_g of the resin continued to increase and approached to the cure temperature, causing the vitrification, i.e. the glass formation, of the epoxy. During the vitrification, the polymerization was inhibited, shifting from a chemical-controlled to a diffusion-controlled process because of the increasing viscosity of the system. As a result, the capacitance underwent a frequency dependent sigmoidal decreasing transition, then, independent of frequency, reached to asymptotic values. The MSP was capable of measuring small changes of capacitance as compared to the LCR meter at the end of the polymerization (See Fig. S5 in Supplementary Material for details). The asymptotic values suggested lack of additional cross-linking that would further restrict the mobility of the dipoles, thus indicating the end of the polymerization. In the meantime, the conductance continued to drop and reached to asymptotic values. The developed MSP could measure a lower value of the conductance for all three experiments as compared to the LCR meter. For instance, in Fig. 7a, the conductance measured by 100 Hz from LCR meter dropped from 1E-9 to 1E–10 S from hour 15 to hour 40, while that measured by the MSP changed from 1E-9 to 1E–12 S.

In summary, along the polymerization, the capacitance from the MSP followed a similar trend to the 1 MHz measurement from the LCR meter. On the other hand, the MSP was capable of measuring lower conductance. Furthermore, the on-board temperature measurement capability complemented the impedance measurements, and furthered the understanding of the polymerization process. To explore the reproducibility and long-term stability of the MSPs for *in situ* monitoring of epoxy polymerization, a set of four MSPs was characterized. Results of reproducibility and long-term stability studies (Supplementary Material Fig. S6) indicate that the responses of the MSPs were consistent over a period of at least nine months. It was observed that the sensors had a relative standard deviation of less than 3% throughout the experiments, and the sensors had approximately the same response after embedded in the fully cured epoxy for 2 days, and for 9 months, respectively.

5. Conclusions

In this work, we designed and fabricated a flexible multifunctional miniaturized sensor patch through flexible printed circuit board fabrication processes, for rapid, localized, stable, and accurate impedance and temperature measurements. The fabrication of the MSP was compatible with flexible printed circuit board technology, allowing facile integration of microcontroller with the developed IDS, and other functional devices for various purposes. Thanks to the integrated microcontroller, the data of various sensors were processed locally and transmitted in a digital form, minimizing the influence of the noise on the data over a long distance. Complex impedance sensing was achieved through the combination of the interdigital sensor and a simple readout circuitry. The developed MSP was integrated in reactive polymers for real time and *in situ* monitoring of their polymerization processes. The MSP clearly indicated the flow-front, curing, end of curing of the polymers, which were confirmed by a commercial impedance analyzer. Our results demonstrate the potential of the proposed sensor patch as an integrated solution for *in situ* and real-time impedance sensing device.

Acknowledgements

The research leading to these results received funding from the Flemish Agency for Innovation by Science and Technology (IWT)–through the program for Strategic Basic Research (SBO) under grant agreement n° 120024(Self Sensing Composites). Y. Yang thanks Dr. Jiu for various fruitful discussions.

Appendix A. Supplementary data

Supplementary data associated with this article can be found, in the online version, at https://doi.org/10.1016/j.snb.2018.01.141.

References

[1] S.L. Swisher, M.C. Lin, A. Liao, E.J. Leeflang, Y. Khan, F.J. Pavinatto, et al., Impedance sensing device enables early detection of pressure ulcers in vivo, Nat. Commun. 6 (2015).
[2] S. Ingebrandt, Bioelectronics: sensing beyond the limit, Nat. Nanotechnol. 10 (2015) 734–735.

[3] T. Yokota, Y. Inoue, Y. Terakawa, J. Reeder, M. Kaltenbrunner, T. Ware, et al., Ultraflexible, large-area, physiological temperature sensors for multipoint measurements, Proc. Natl. Acad. Sci. 112 (2015) 14533–14538.
[4] Y.C. Lai, J. Deng, S.L. Zhang, S. Niu, H. Guo, Z.L. Wang, Single–Thread–Based wearable and highly stretchable triboelectric nanogenerators and their applications in cloth–based self–powered human–interactive and biomedical sensing, Adv. Funct. Mater. 27 (2017).
[5] B.J. Leever, C.A. Bailey, T.J. Marks, M.C. Hersam, M.F. Durstock, In situ characterization of lifetime and morphology in operating bulk heterojunction organic photovoltaic devices by impedance spectroscopy, Adv. Energy Mater. 2 (2012) 120–128.
[6] P.A. Troshin, D.K. Susarova, Y.L. Moskvin, I.E. Kuznetsov, S.A. Ponomarenko, E.N. Myshkovskaya, et al., Impedance measurements as a simple tool to control the quality of conjugated polymers designed for photovoltaic applications, Adv. Funct. Mater. 20 (2010) 4351–4357.
[7] B. Zhang, Z. Xiang, S. Zhu, Q. Hu, Y. Cao, J. Zhong, et al., Dual functional transparent film for proximity and pressure sensing, Nano Res. 7 (2014) 1488.
[8] Y.C. Lai, B.W. Ye, C.F. Lu, C.T. Chen, M.H. Jao, W.F. Su, et al., Extraordinarily sensitive and low-voltage operational cloth-based electronic skin for wearable sensing and multifunctional integration uses: a tactile-induced insulating-to-conducting transition, Adv. Funct. Mater. 26 (8) (2016) 1286–1295.
[9] H. Gullapalli, V.S. Vemuru, A. Kumar, A. Botello-Mendez, R. Vajtai, M. Terrones, et al., Flexible piezoelectric ZnO–paper nanocomposite strain sensor, Small 6 (2010) 1641–1646.
[10] Y. Yang, S. Ding, T. Araki, J. Jiu, T. Sugahara, J. Wang, et al., Facile fabrication of stretchable Ag nanowire/polyurethane electrodes using high intensity pulsed light, Nano Res. 9 (2016) 401–414.
[11] S.L. Zhang, Y.C. Lai, X. He, R. Liu, Y. Zi, Z.L. Wang, Auxetic foam-based contact-mode triboelectric nanogenerator with highly sensitive self-powered strain sensing capabilities to monitor human body movement, Adv. Funct. Mater. 27 (25) (2017), 1606695.
[12] P. Schubel, R. Crossley, E. Boateng, J. Hutchinson, Review of structural health and cure monitoring techniques for large wind turbine blades, Renew. Energ. 51 (2013) 113–123.
[13] Y. Yang, G. Chiesura, T. Vervust, F. Bossuyt, G. Luyckx, J. Degrieck, et al., Design and fabrication of a flexible dielectric sensor system for in situ and real-time production monitoring of glass fibre reinforced composites, Sens. Actuators A 243 (2016) 103–110.
[14] M. Aicher, H. Grothe, B. Wolf, A novel thin film impedance Ca ion sensor for drinking water, Sens. Actuators B 244 (2017) 1103–1112.
[15] F. Schipani, D. Miller, M. Ponce, C. Aldao, S. Akbar, P. Morris, et al., Conduction mechanisms in SnO 2 single-nanowire gas sensors: an impedance spectroscopy study, Sens. Actuators B 241 (2017) 99–108.
[16] C.C. Mayorga-Martinez, A. Ambrosi, A.Y.S. Eng, Z. Sofer, M. Pumera, Metallic 1T-WS2 for selective impedimetric vapor sensing, Adv. Funct. Mater. 25 (2015) 5611–5616.
[17] Y. Yang, G. Chiesura, G. Luyckx, T. Vervust, F. Bossuyt, J. Vanfleteren, et al., In situ on-line cure monitoring of composites by embedded interdigital sensor, 16th European Conference on Composite Materials (ECCM-16) (2014).
[18] Y. Yang, G. Chiesura, G. Luyckx, T. Vervust, F. Bossuyt, M. Kaufmann, et al., Development of a dielectric sensor system for the on-line cure monitoring of composites, Procedia Technol. 15 (2014) 631–637.
[19] C. Yang, S.R. Jadhav, R.M. Worden, A.J. Mason, Compact low-power impedance-to-digital converter for sensor array microsystems, IEEE J. Solid-St. Circ. 44 (2009) 2844–2855.
[20] A. Manickam, A. Chevalier, M. McDermott, A.D. Ellington, A. Hassibi, A CMOS electrochemical impedance spectroscopy (EIS) biosensor array, IEEE Trans. Biomed. Circuits Syst. 4 (2010) 379–390.
[21] H. Jafari, L. Soleymani, R. Genov, 16-channel CMOS impedance spectroscopy DNA analyzer with dual-slope multiplying ADCs, IEEE Trans. Biomed. Circ. Syst. 6 (2012) 468–478.
[22] M. Bakhshiani, M.A. Suster, P. Mohseni, A broadband sensor interface IC for miniaturized dielectric spectroscopy from MHz to GHz, IEEE J. Solid-St. Circ. 49 (2014) 1669–1681.
[23] K. Alkin, T. Stockinger, M. Zirkl, B. Stadlober, S. Bauer-Gogonea, M. Kaltenbrunner, et al., Paper-based printed impedance sensors for water sorption and humidity analysis, Flexible Printed Electron. 2 (2017) 014005.
[24] M. Kaltenbrunner, T. Sekitani, J. Reeder, T. Yokota, K. Kuribara, T. Tokuhara, et al., An ultra-lightweight design for imperceptible plastic electronics, Nature 499 (2013) 458–463.
[25] H. Li, K.W. Jung, Z.D. Deng, Piezoelectric transducer design for a miniaturized injectable acoustic transmitter, Smart Mater. Struct. 24 (2015) 115010.
[26] C. Dias, R. Igreja, A method of recursive images to obtain the potential, the electric field and capacitance in multi-layer interdigitated electrode (IDE) sensors, Sens. Actuators A 256 (2017) 95–106.
[27] H.P. Hsu, R. Ranjan, Signals and Systems, McGraw-Hill, 2014.
[28] Y. Yang, G. Chiesura, T. Vervust, J. Degrieck, J. Vanfleteren, Design and fabrication of a shielded interdigital sensor for noninvasive In situ real-time production monitoring of polymers, J. Polym. Sci. Part B: Polym. Phys. 54 (20) (2016) 2028–2037.
[29] M. Günthel, J. Hübscher, R. Dittrich, E. Weber, Y. Joseph, F. Mertens, XPS and resistive studies on thin films of a copper (II)-based coordination polymer deposited on functionalized interdigital electrodes, J. Polym. Sci. Part B: Polym. Phys. 53 (2015) 335–344.
[30] J. Jiang, X. Wang, R. Chao, Y. Ren, C. Hu, Z. Xu, et al., Smartphone based portable bacteria pre-concentrating microfluidic sensor and impedance sensing system, Sens. Actuators B 193 (2014) 653–659.
[31] M. Urbiztondo, I. Pellejero, A. Rodriguez, M. Pina, J. Santamaria, Zeolite-coated interdigital capacitors for humidity sensing, Sens. Actuators B 157 (2011) 450–459.
[32] J. Vanfleteren, M. Gonzalez, F. Bossuyt, Y.Y. Hsu, T. Vervust, I. De Wolf, et al., Printed circuit board technology inspired stretchable circuits, MRS Bull. 37 (2012) 254–260.
[33] A. de la Vega, J.Z. Kovacs, W. Bauhofer, K. Schulte, Combined Raman and dielectric spectroscopy on the curing behaviour and stress build up of carbon nanotube–epoxy composites, Compos. Sci. Technol. 69 (2009) 1540–1546.
[34] D. Karalekas, J. Cugnoni, J. Botsis, Monitoring of process induced strains in a single fibre composite using FBG sensor: a methodological study, Compos Part A 39 (2008) 1118–1127.
[35] N. Sbirrazzuoli, A. Mititelu-Mija, L. Vincent, C. Alzina, Isoconversional kinetic analysis of stoichiometric and off-stoichiometric epoxy-amine cures, Thermochim. Acta 447 (2006) 167–177.
[36] A. Serghei, M. Tress, J. Sangoro, F. Kremer, Electrode polarization and charge transport at solid interfaces, Phys. Rev. B 80 (2009) 184301.

Biographies

Yang Yang obtained his Ph.D. degree in electrical engineering from Ghent University, Ghent, Belgium, in 2017. From 2011 to 2012, he was with Philips Innovation Center as a software designer. His current main research interests are flexible and stretchable sensor systems.

Ke Xu obtained his Master's Degree in electrical engineering from Ghent University in 2016. His current main research interests are flexible and stretchable sensor systems.

Thomas Vervust received the Master's degree in electronics engineering and the Ph.D. degree in stretchable and washable electronics for embedding in textiles from Ghent University, Ghent, Belgium, in 2007 and 2012, respectively. He is a Research Scientist with the Center for Microsystems Technology (CMST), Ghent University, (affiliated with IMEC). His current research interests the development of stretchable electronic technologies for large area applications.

Jan Vanfleteren (M'11) received the Ph.D. degree in electronic engineering from Ghent University, Ghent, Belgium, in 1987. He is currently a Senior Engineer with the IMEC-CMST Group and a part time Professor with Ghent University. He has co-authored over 200 papers in international journals and conferences and holds 14 patents/patent applications. His current research interests include the development of novel interconnection, assembly and substrate technologies, especially for wearable and implantable electronics and sensor applications. Dr. Vanfleteren is a member of IMAPS, IEEE and MRS.